Aim2 Deficiency Ameliorates Lacrimal Gland Destruction and Corneal Epithelium Defects in an Experimental Dry Eye Model

Yu Chen,[1] Jiheng Pu,[1,3] Xinda Li,[1] Lili Lian,[1,2] Chaoxiang Ge,[1,2] Zuimeng Liu,[1] Weizhuo Wang,[1] Ling Hou,[1] Wei Chen,[1,2] and Jinyang Li[1,2]

[1]State Key Laboratory of Ophthalmology, Optometry and Visual Science, Eye Hospital, Wenzhou Medical University, Wenzhou, China
[2]National Clinical Research Center for Ocular Diseases, Eye Hospital, Wenzhou Medical University, Wenzhou, China
[3]Department of Ophthalmology, The East Beijing Medical Center of Chinese PLA General Hospital, Beijing, China

Correspondence: Wei Chen, Eye Hospital and School of Ophthalmology and Optometry, Wenzhou Medical University, 270 West Xueyuan Road, Wenzhou, Zhejiang 325027, China; chenweimd@wmu.edu.cn.
Jinyang Li, Eye Hospital and School of Ophthalmology and Optometry, Wenzhou Medical University, 270 West Xueyuan Road, Wenzhou, Zhejiang 325027, China; lijinyang@eye.ac.cn.

YC and JP contributed equally to the work presented here and should therefore be regarded as equivalent authors.

Received: September 27, 2022
Accepted: February 20, 2023
Published: March 15, 2023

Citation: Chen Y, Pu J, Li X, et al. *Aim2* deficiency ameliorates lacrimal gland destruction and corneal epithelium defects in an experimental dry eye model. *Invest Ophthalmol Vis Sci.* 2023;64(3):26. https://doi.org/10.1167/iovs.64.3.26

Purpose. Dry eye disease (DED) is a multifactorial disease that is associated with inflammation. Excessive DNA is present in the tear fluid of patients with DED. Absent in melanoma 2 (AIM2) is a key DNA sensor. This study aimed to investigate the role of AIM2 in the pathogenesis of DED.

Methods. DED was induced by injection of scopolamine (SCOP). Aberrant DNA was detected by cell-free DNA (cfDNA) ELISA and immunostaining. Corneal epithelial defects were assessed by corneal fluorescein staining, zonula occludens-1 immunostaining and TUNEL. Tear production was analyzed by phenol red thread test. Lacrimal gland (LG) histology was evaluated by hematoxylin and eosin staining, and transmission electron microscopy examination. Macrophage infiltration in LG was detected by immunohistochemistry for the macrophage marker F4/80. Gene expression was analyzed by RT-qPCR. Protein production was examined by immunoblot analysis or ELISA.

Results. *Aim2*$^{-/-}$ mice displayed a normal structure and function of LG and cornea under normal conditions. In SCOP-induced DED, wild type (WT) mice showed increased cfDNA in tear fluid, and aberrant accumulations of dsDNA accompanied by increased AIM2 expression in the LG. In SCOP-induced DED, WT mice displayed damaged structures of LG, reduced tear production, and severe corneal epithelium defects, whereas *Aim2*$^{-/-}$ mice had a better preserved LG structure, less decreased tear production, and improved clinical signs of dry eye. Furthermore, genetic deletion of *Aim2* suppressed the increased infiltration of macrophages and inhibited N-GSDMD and IL18 production in the LG of SCOP-induced DED.

Conclusions. *Aim2* deficiency alleviates ocular surface damage and LG inflammation in SCOP-induced DED.

Keywords: dry eye disease, absent in melanoma, inflammasome, lacrimal gland, macrophage

Dry eye disease (DED) is a multifactorial disease of the ocular surface characterized by a loss of homeostasis of the tear film, accompanied by ocular symptoms, including discomfort or visual disturbances.[1] Several findings have provided evidence that inflammasomes are actively involved in DED pathogenesis.[2–5] Inflammasomes are multiprotein complexes formed within the cytosol following the detection of pathogen-associated molecular patterns, damage-associated molecular patterns, and homeostasis-altering molecular processes, and they play critical roles in the development of inflammatory conditions.[6–9]

Inflammasome activation requires recognition of ligand by sensor proteins such as NLRP3 and Absent in melanoma 2 (AIM2), followed by the recruitment of the adaptor protein, apoptosis speck-like protein (ASC), and the activation of caspase-1, which subsequently promotes the processing of pro-IL-1β and pro-IL-18 into a mature form, as well as a gasdermin-D (GSDMD)–mediated form of programmed cell death, commonly known as *pyroptosis*.[7,10,11] Pyroptosis was found to be involved in dry eye, displayed as the elevation of its executor GSDMD N-terminal domain (N-GSDMD) in the tears of patients with DED.[3] Moreover, GSDMD deficiency alleviates desiccating stress-induced corneal epithelium defects, which suggests that GSDMD-driven pyroptosis contributes to the pathogenesis of DED.[2]

AIM2 inflammasome is one of the upstream inflammasomes of GSDMD.[9,12] AIM2 belongs to the PYHIN family, which contains pyrin and HIN domain.[13] Different from other sensor proteins of inflammasomes, AIM2 can detect and bind to aberrant cytosolic double-stranded DNA, subsequently activating inflammasome.[14,15] The AIM2 inflammasome is essential for host defense against bacterial and

viral pathogens.[16] Owing to the lack of sequence specificity recognized by AIM2, it cannot distinguish between microbial DNA and aberrant self-DNA.[17] Therefore the activation of AIM2 in response to self-DNA has important implications in immunity. Emerging evidence has indicated that AIM2 can sense DNA damage from cellular stress during neurodevelopment or cell-free DNA after acute tissue injuries and chemotherapeutic agent treatment and subsequently recruits ASC and activates caspase-1, finally leading to mature IL-1β and IL-18 secretion and GSDMD-mediated pyroptosis.[18–20] However, it remains unclear whether AIM2 inflammasome is involved in the development of DED.

It has been shown that excessive extracellular DNA is present in the tear fluid of patients with DED and correlates with signs and symptoms in tear-deficient DED subtypes.[21,22] Given that AIM2 could be activated by both intracellular and extracellular DNA that access the cytosol by phagocytic cells, such as macrophages or by exosome delivery,[20,23,24] we propose that the AIM2 inflammasome might be activated by aberrant DNA in DED and contributes to the development of DED. To validate this hypothesis, we evaluated the aberrant DNA in tear fluid and lacrimal gland (LG), and further examined the expression change of *Aim2* in LG, cornea and conjunctiva of experimental DED. Furthermore, we used *Aim2*-deficient mice (termed *Aim2*$^{-/-}$)[16] to elucidate the roles of AIM2 in the pathological process of DED and explore the underlying mechanisms.

Material and Methods

Mice

Experimental mice were bred in the SPF facility of Wenzhou Medical University, and the animal care and experimental procedures were performed in compliance with the ARVO statements on the Use of Animals in Ophthalmic and Vision Research, and this study was approved by the Experimental Animal Ethics Committee of Wenzhou Medical University (xmsq2021-0193). C57BL/6 J mice were purchased from Charles River Laboratories of China, and *Aim2*$^{-/-}$ mice were purchased from Jackson laboratory (Stock Number: 013144). 6- to 8-week-old female C57BL/6 J mice and *Aim2*$^{-/-}$ mice were used in experiments.

Experimental Dry Eye Model

Experimental DED was induced in mice by subcutaneously injection of scopolamine hydrobromide (SCOP, 0.5 mg/0.2 mL in sterile saline solution; Sigma-Aldrich Corp., St. Louis, MO, USA) three times a day (9 AM, 1 PM, and 5 PM) alternating between the right and left flanks of eight-week-old female mice for a total of five days. Control mice were injected with sterile saline solution.

Corneal Fluorescein Staining (CFS)

To examine CFS, 0.5 µL of 2.5 % fluorescein was applied into the lateral conjunctival sac of the mice. After three minutes, corneas were evaluated with a slit-lamp microscope under a cobalt blue light. Punctuate epithelial staining was recorded in a masked manner according to the National Eye Institute grading system, scoring 0 to 3 for each of five areas of the cornea: central, superior, inferior, nasal, and temporal.[25]

Histology, Immunohistochemistry, Periodic Acid Schiff (PAS) Staining and Goblet Cell Measurement

The extraorbital LGs were surgically excised, fixed in 10% formalin overnight, and embedded in paraffin, and 5 µm sections were cut. Sections were stained with hematoxylin and eosin for evaluation of morphology.

For immunohistochemistry, lacrimal gland sections were deparaffinized, rehydrated. Heat-mediated antigen retrieval was performed using Powerful Antigen Retrieval Solution (Beyotime Institute of Biotechnology, Jiangsu, China). The samples were incubated overnight at 4°C with specific primary antibodies anti-F4/80 (1:250; Cell Signaling Technology, Danvers, MA, USA) and detected using a horseradish peroxidase–conjugated compact polymer system (Beyotime Institute of Biotechnology). DAB was used as the chromogen. Hematoxylin was used as a counterstain. The area percentages of F4/80 positive cells were quantified in three random vision fields of one sample (1 sample = 1 mouse) using ImageJ software. Five mice/group were analyzed for comparison of macrophage infiltration between wild type (WT) and *Aim2*$^{-/-}$ mice under normal conditions. Four mice/group were analyzed for comparison among WT control, WT SCOP, and *Aim2*$^{-/-}$ SCOP groups.

For PAS staining, the eyes with surrounding eyelids were fixed in 10% formalin overnight and embedded in paraffin. Section 5 µm thick were cut from each sample. The sections were deparaffinized and stained with PAS staining kit (Solarbio Life Science, Beijing, China) for identification of goblet cells. The number of positively stained goblet cells in the inferior conjunctiva was measured.

Transmission Electron Microscopy

The fresh LG tissue of mice was cut into small pieces and fixed with 2.5% glutaraldehyde buffer solution overnight at 4°C. After rinsing the samples in PBS buffer, samples were dehydrated with gradient ethanol, embedded in resin, and thin-sectioned using an ultramicrotome (RMC Boeckeler Instruments, Inc., Tucson, AZ, USA). Ultrathin sections were stained with uranyl acetate and photographed using transmission electron microscope (Hitachi, Tokyo, Japan).

Tear Volume Measurement

The amount of tear was measured with the phenol red thread tear test. Briefly, cotton threads (Tianjin Jingming New Technological Development Co., Ltd., Tianjin, China) was held in the lateral conjunctival sac of each eye for 15 seconds. A color change from yellow to red occurs in the thread when tears are absorbed. The wet (red) portion was measured.

Measurement of Cell-Free DNA (cf DNA) Abundance in Tear Fluid

Tear fluid (1 µL) was collected from the lower lid margin of the mice. Because SCOP mice show severe tear deficiency, a drop of 1 µL preservative-free artificial tears was instilled in the eye, and conjunctival washings were collected. One sample consisted of tear washing from both eyes of one mouse, pooled (2 µL) + 0.1% BSA (8 µL), spun in a centrifuge for 10 minutes at 3000 *g* (Eppendorf centrifuge, 5427R) and

Investigative Ophthalmology & Visual Science

the supernatant was stored at −80°C until the assay was performed. Cell-free DNA (cfDNA) abundance was detected using mouse cfDNA ELISA kit (Shanghai Jun Yu Biotechnology, Shanghai, China). ELISA was performed as follows: samples were diluted to 50 µL and added to wells coated with anti-mouse cfDNA antibodies. Horseradish peroxidase–conjugated antibody (100 µL) was added to the wells and incubated for one hour at 37°C. After washing, the TMB (3, 3′,5,5′-tetramethylbenzidine Chromogen Solution was added to the wells and incubated for 15 minutes. Stop Solution was added to each well to terminate the reaction. Absorbance was read at 450 nm by a full-wavelength microplate reader (SpectraMax190; Molecular Devices, San Jose, CA, USA). The concentration of cfDNA was calibrated from a dose-response curve based on the reference standards. The calculated concentration was multiplied by the dilution rate of tear fluid to obtain the final concentration.

Immunostaining

Cryostat sections (10 µm) of LGs fixed in 4% paraformaldehyde for 15 minutes. After rinsing, the sections were blocked with 3% bovine serum albumin for one hour at room temperature. The samples were incubated overnight at 4°C with specific primary antibodies anti-dsDNA (1:200, MAB1293; Sigma-Aldrich Corp.). The staining was revealed by secondary antibodies Alexa Fluor 488 (1:200; Life Technologies, Carlsbad, CA, USA). To avoid interference of nonspecific autofluorescent signals in LG that were excited at all wavelengths, sections were examined by confocal microscopy using light at 488, and 561 nm for excitation. The signals that only exist at 488 excitation wavelength were considered as specific signals and used in the results. Meanwhile, PBS was used as negative control instead of anti-dsDNA primary antibody during the immunostaining.

Whole mounts of cornea were fixed with methanol on ice for 10 minutes. After blocking with 3% bovine serum albumin for 30 minutes, the samples were incubated with primary antibodies of anti-ZO-1 (1:200, Invitrogen, Carlsbad, CA, USA) overnight at 4°C. The staining was revealed by secondary antibodies Alexa Fluor 594 (1:200; Life Technologies). Immunostaining results were observed and photographed on a Zeiss confocal microscope (Zeiss, Oberkochen, Germany).

TUNEL Staining

Cryopreserved corneal sections were prepared and TUNEL staining was performed using a TUNEL Kit (Roche, Basel, Switzerland), according to the instructions. In brief, frozen sections of mouse corneas were permeabilized with 0.1% Triton X-100, 0.1% sodium citrate for two minutes on ice. Then the corneal samples were incubated in a TUNEL reaction mixture for one hour at 37°C. Images were obtained on a Zeiss confocal microscope.

Western Blotting

Proteins were extracted from LG tissues using protein lysis solution supplemented with proteinase and phosphatase inhibitors (Beyotime Institute of Biotechnology). Equivalent amounts of protein extracts were loaded and separated on 10% to 15% SDS-PAGE gels, and then transferred to nitrocellulose membranes (Whatman PLC, Maidstone, UK). The membranes were probed with primary antibodies as follows: anti-ASC (1:500, Santa Cruz Biotechnology, sc-514414), anti-pro Caspase-1+P10+P12 (1:1000, ab179515; Abcam, Cambridge, MA, USA), anti-GSDMD (1:1000, Abcam, ab219800), anti-IL-1β (1:500, AF-401NA; R&D Systems, Minneapolis, MN, USA), anti-IL-18 (1:500, ab71495; Abcam), β–actin (1:2000, 4967s; Cell Signaling Technology). After incubation at 4°C overnight, the primary antibodies were revealed with the appropriate fluorescein-conjugated secondary antibodies (LI-COR Biosciences, Lincoln, NE, USA) at room temperature for two hours in the dark. The protein bands were scanned using the odyssey CLx system (LI-COR Biosciences), and quantitative densitometry of the bands was performed using ImageJ software.

ELISA

The levels of IL-1β and IL-18 inflammatory factors in LG lysates were detected using mouse IL-1β ELISA kit and IL-18 ELISA kit (Multi Sciences Biotech Co. Ltd., Hangzhou, China). ELISA was performed according to the manufacturer's instructions. Absorbance was read at 450 nm with a reference wavelength of 570 nm by a full-wavelength microplate reader (SpectraMax190).

RNA Isolation and RT-qPCR Analysis

Total RNA was extracted from LG, cornea, and conjunctiva using the RNA purification kit (RNeasy Mini Kit; Qiagen, Hilden, Germany) and reverse transcribed into cDNA using random primer and M-MLV reverse transcriptase (Promega Corporation, Madison, WI, USA). Real-time PCR was performed in triplicate with Power SYBR Green PCR Master Mix on a 7500 Real-Time PCR Detection System (Applied Biosystems, Foster City, CA, USA). Relative mRNA expression levels were normalized to Gapdh and analyzed using the $2^{-\Delta\Delta Ct}$ method. Primers used in quantitative PCR are listed in Supplementary Table S1.

Statistical Analysis

Data are presented as the mean ± SD. All experiments are representative of at least three independent experiments. Data were analyzed using GraphPad Prism version 9.0 (GraphPad Software, San Diego, CA, USA). Because laboratory mice are reared in controlled environments and can be considered normal or approximate normal data, Student's *t*-test was used to make comparisons between two groups. One-way ANOVA testing was used to make comparisons among three groups, followed by the Sidak post-hoc test. $P < 0.05$ was considered statistically significant.

Results

Aberrant DNA Accumulations Accompanied by Increased AIM2 Expression in the Lacrimal Gland in SCOP-Induced DED

SCOP is a tropane alkaloid that antagonizes muscarinic activity, which can decrease tear production to induce symptoms of dry eye.[26,27] We induced a murine dry eye model by administering SCOP. After SCOP injection for five days, WT mice displayed severe corneal epithelial damage compared to the control group as seen by fluorescein staining (Figs. 1A, 1B).

Investigative Ophthalmology & Visual Science

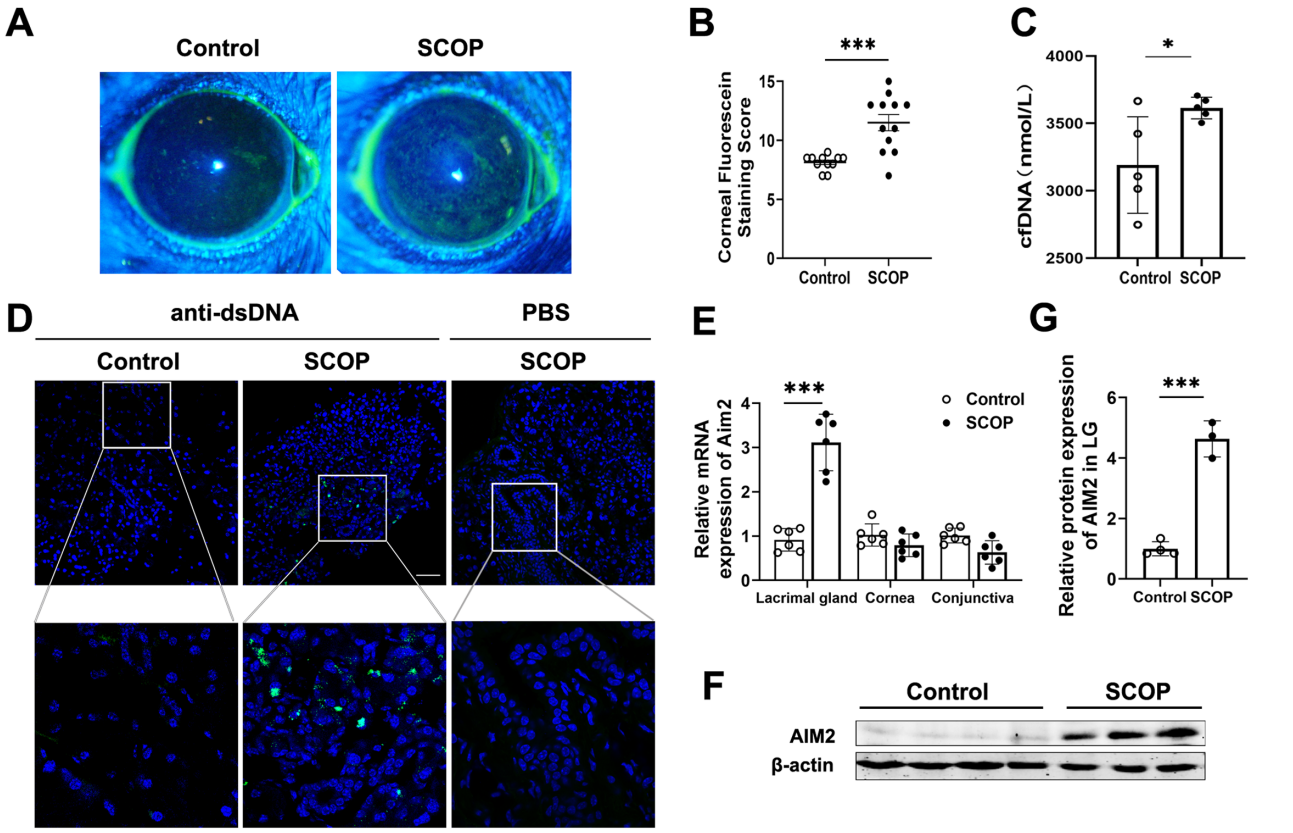

Figure 1. Aberrant DNA accumulations accompanied by increased *Aim2* expression in the lacrimal gland in SCOP-induced DED. Mice were administered with SCOP for five days to induce dry eye, with saline solution used as a control. (**A**) Representative images of corneal fluorescein staining. (**B**) Corneal epithelial damage assessed by standard corneal fluorescein staining scores of control group (n = 11) and SCOP group (n = 12). (**C**) Analysis of cfDNA abundance in tear fluid of control and SCOP group by ELISA (n = 5). (**D**) Representative confocal immunofluorescence images of DNA staining using anti-dsDNA antibody (*green*) in the lacrimal gland of control and SCOP mice. PBS was used as negative control instead of anti-dsDNA primary antibody during the immunostaining. (**E**) Relative fold of *Aim2* transcript in lacrimal gland, cornea and conjunctiva of control group and SCOP group by real-time PCR (n = 6). $^{*}P < 0.05$, $^{***}P < 0.001$. ns, not significant. Immunoblot analysis (**F**) and quantification of band intensity (**G**) of AIM2 and β-actin (protein loading control) in lacrimal glands of the WT control (n = 4), WT SCOP group (n = 3). Control group was taken as the calibrator. $^{***}P < 0.001$.

To confirm whether this DED mouse model is comparable to patients with DED who have excessive DNA in tear fluid,[21,22] cfDNA in tear fluid from the SCOP-induced DED model was examined. As shown in Figure 1C, cfDNA was elevated in tear fluid from the SCOP-induced DED model. The cfDNA in tear fluid might be released from LG and dead corneal epithelial cells in SCOP-induced DED. We further examined aberrant DNA in the LG of SCOP-induced DED by immunostaining with dsDNA antibody. As shown in Figure 1D, there was noticeable aberrant DNA in the LG of the SCOP group.

The mRNA levels of *Aim2* were evaluated in LG, cornea and conjunctiva of SCOP-induced DED. Compared with control, SCOP mice showed a significant increase in *Aim2* mRNA level in the LG (Fig. 1E). We further analyzed the expression of AIM2 protein in the LG, and found that AIM2 protein level increased significantly in the LG of SCOP-induced DED model (Figs. 1F, 1G).

AIM2 Is Not Essential for Ocular Surface and LG Homeostasis in Normal Conditions

To investigate the contribution of increased *Aim2* to the dry eye process, we first evaluated the role of AIM2 in ocular surface homeostasis by comparing ocular surface alterations between *Aim2*−/− and WT mice under normal conditions. Corneal fluorescein staining was used to evaluate corneal epithelial defects. According to the grading standards, there was no significant difference in corneal fluorescein scores between WT and *Aim2*$^{-/-}$ mice (Fig. 2A, B). Furthermore, the immunofluorescence images of zonula occludens-1 (ZO-1) revealed similar corneal integrity in *Aim2*$^{-/-}$ mice as compared to WT mice (Fig. 2C). The PAS staining of conjunctival goblet cells showed comparable cell densities in WT and *Aim2*$^{-/-}$ mice (Figs. 2D, 2E).

We further investigated whether AIM2 deficiency affects the histology and function of the LG under normal conditions. Macroscopically, we observed a comparable appearance and weight of *Aim2*$^{-/-}$ LGs compared with WT at eight weeks of age (Fig. 3A, B). The LGs of *Aim2*$^{-/-}$ mice exhibited normal morphology of the acini and ducts (Fig. 3C). Moreover, transmission electron microscopy analysis of LGs from *Aim2*$^{-/-}$ mice showed the cytoplasm of acinar cells filled with secretory granules (SG), similar to WT (Fig. 3D). To determine whether *Aim2*$^{-/-}$ mouse LGs have secretory activity comparable to that of WT mice, tear production was measured using the phenol red cotton thread technique. No significant difference was found in tear production in

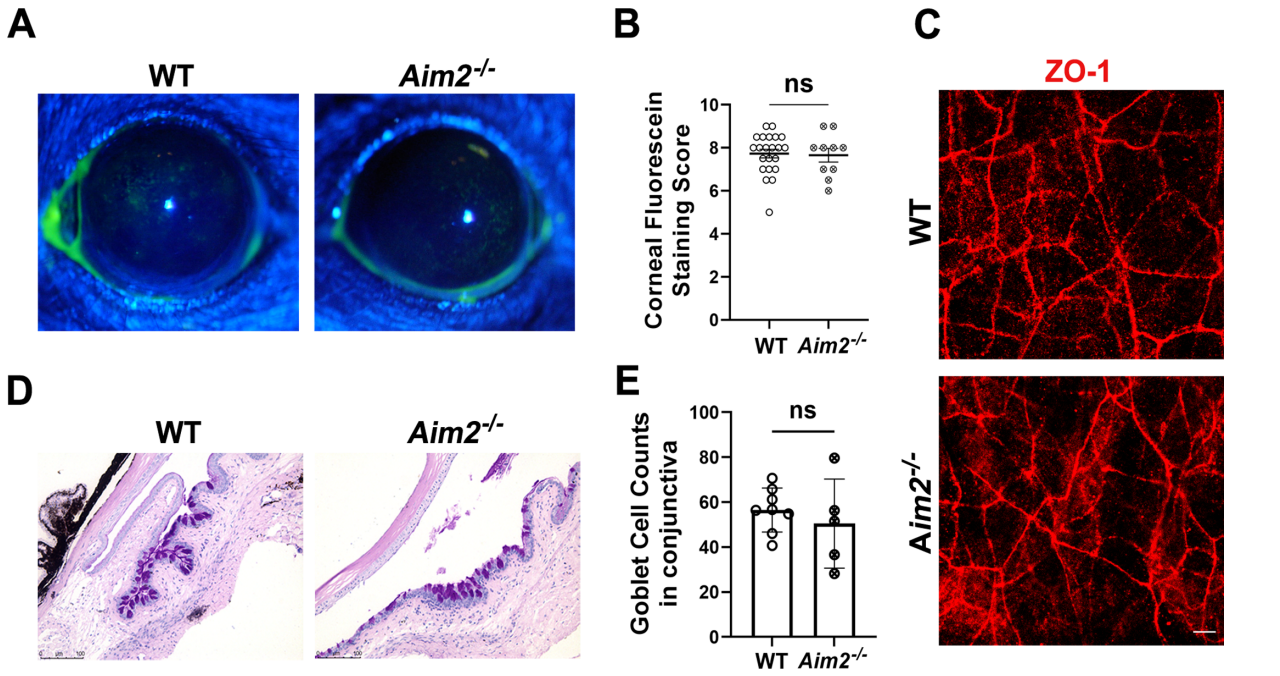

Figure 2. *Aim2* deficiency does not influence ocular surface phenotype under normal conditions. (**A**) Representative images of corneal fluorescein staining of WT and *Aim2*$^{-/-}$ mice. (**B**) Corneal fluorescein staining score analysis of WT (n = 22) and *Aim2*$^{-/-}$ mice (n = 10). (**C**) Representative images of whole mounts of cornea immunostained for ZO-1 (*red*). *Scale bar*: 5 µm. (**D**) Representative images of the inferior conjunctival sections stained with PAS. *Scale bar*: 100 µm. (**E**) The numbers of positively PAS-stained goblet cells in the inferior conjunctiva of WT (n = 8) and *Aim2*$^{-/-}$ mice (n = 5) was measured. ns, not significant.

Aim2$^{-/-}$ mice compared to WT mice (Figs. 3E, 3F). RT-qPCR was performed to evaluate the expression of *Aim2* and other key regulators of the AIM2 inflammasome pathway in the LG of WT and *Aim2*$^{-/-}$ mice. As shown in Figure 3G, *Aim2* expression was almost absent, whereas the expression of *Asc, Casp1, Il1β, Il18* and *Gsdmd* remained at similar levels in the LG of *Aim2*$^{-/-}$ mice. We further analyzed IL-1β and IL-18 protein levels in the LG of non-treated WT and *Aim2*$^{-/-}$ mice by ELISA. The results showed that similar levels of IL-1β and IL-18 were present in the LG of non-treated WT and *Aim2*$^{-/-}$ mice (Fig. 3H).

Genetic Deletion of AIM2 Alleviates Corneal Epithelium Defects in SCOP-Induced DED

Corneal epithelial barrier disruption is an important indicator of the severity of DED. To determine the specific contribution of AIM2 in DED, we evaluated the ocular surface phenotypes of the *Aim2*$^{-/-}$ dry eye model. After the administration of SCOP for 5 days, WT mice showed severe punctate epithelial erosion in the cornea; however, *Aim2*$^{-/-}$ mice showed significantly lower corneal fluorescein staining scores (Figs. 4A, 4B). Furthermore, the disrupted corneal epithelial tight junction protein ZO-1 in SCOP-induced DED was largely restored by *Aim2* deficiency (Fig. 4C). The TUNEL assay was performed to evaluate the apoptosis of corneal epithelial cells. Consistent with corneal epithelial barrier destruction, the WT SCOP group displayed an increased percentage of TUNEL-positive apoptotic corneal epithelial cells, whereas the *Aim2*$^{-/-}$ SCOP group showed a lower percentage of apoptotic cells (Figs. 4D, 4E).

Aim2 Deficiency Ameliorates LG Destruction and Secretory Dysfunction in SCOP-Induced Dry Eye Model

The LG is the main source of aqueous tears, and inadequate production of aqueous tears leads to signs of dry eye.[28,29] To address the concern of whether deletion of AIM2 ameliorates the dry eye phenotype in the cornea through the protection of the structure and function of LGs in SCOP-induced DED, we performed functional and histological analysis of LGs. Aqueous tear production measurements using phenol red cotton-thread revealed that SCOP significantly inhibited tear secretion, whereas *Aim2* deletion markedly attenuated the extent of tear reduction (Figs. 5A, 5B). To further investigate the changes in LG structure, we evaluated the LGs macroscopically and microscopically. Compared to the control group, the LGs in the WT SCOP group displayed decreased size and weight. However, the LGs in the *Aim2*$^{-/-}$ SCOP group showed alleviated extent of size and weight decrease (Figs. 5C, 5D). We further microscopically analyzed the LG structure. We observed acinar atrophy in the LGs of WT SCOP group, whereas the LGs of *Aim2*$^{-/-}$ SCOP group exhibited much better preservation of structure and had more normal-appearing acini (Fig. 5E). The ultrastructural morphological features of the acinar cells were examined using transmission electron microscopy. As shown in Figure 5F, acinar cells in control LGs showed a very dense endoplasmic reticulum network, and the cytoplasm was filled with SGs, whereas the acinar cells in WT SCOP group exhibited few SGs. Compared with WT SCOP group, the acinar cells in *Aim2*$^{-/-}$ SCOP group showed more SGs.

Investigative Ophthalmology & Visual Science

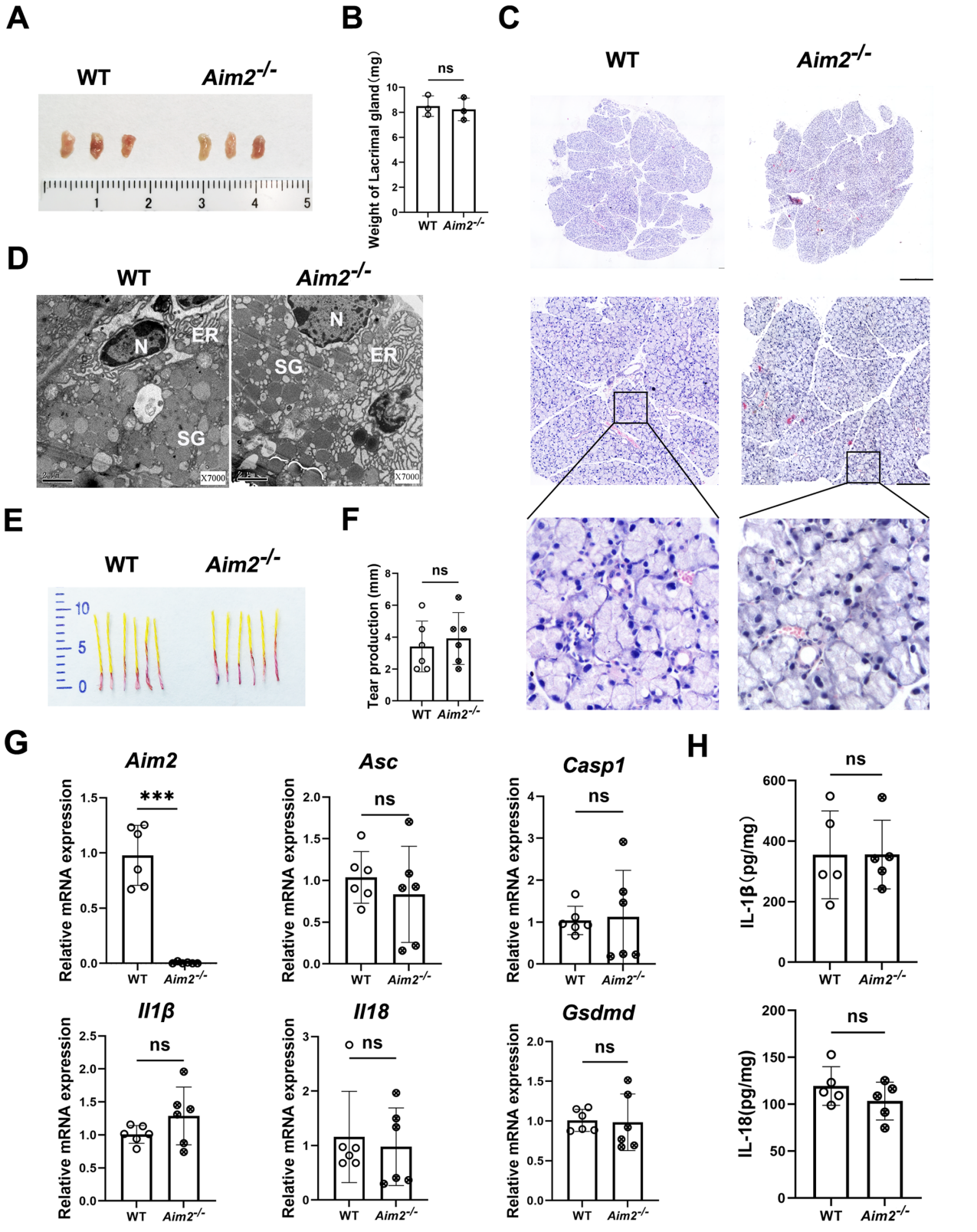

Figure 3. *Aim2* deficiency does not affect histology and function of lacrimal gland. (**A**) Macro images of lacrimal glands in WT and *Aim2*$^{-/-}$ mice. (**B**) Comparison of lacrimal gland weight in WT and *Aim2*$^{-/-}$ mice (n = 3). (C) Representative images of hematoxylin and eosin–stained lacrimal glands sections in WT and *Aim2*$^{-/-}$ mice. *Scale bar* of images in the upper row: 500 µm. *Scale bar* of images in the middle row: 200 µm. (**D**) Representative transmission electron microscopy images of lacrimal glands in WT and *Aim2*$^{-/-}$ mice. N, nuclei; ER, endoplasmic reticulum; SG, secretory granules. (**E**) Aqueous tear production analysis by phenol red thread test in WT and *Aim2*$^{-/-}$ mice (n = 6). (**F**) Quantification of the tear production by the length of wet (*red*) portion of thread in **E**. (**G**) Quantitative gene analysis of mRNA transcripts in lacrimal gland of WT and *Aim2*$^{-/-}$ mice by real-time PCR (n = 6). ***$P < 0.001$. ns, not significant. (**H**) Analyses of IL-1β and IL-18 in the lacrimal glands of WT and *Aim2*$^{-/-}$ mice by ELISA (n = 5). ns, not significant.

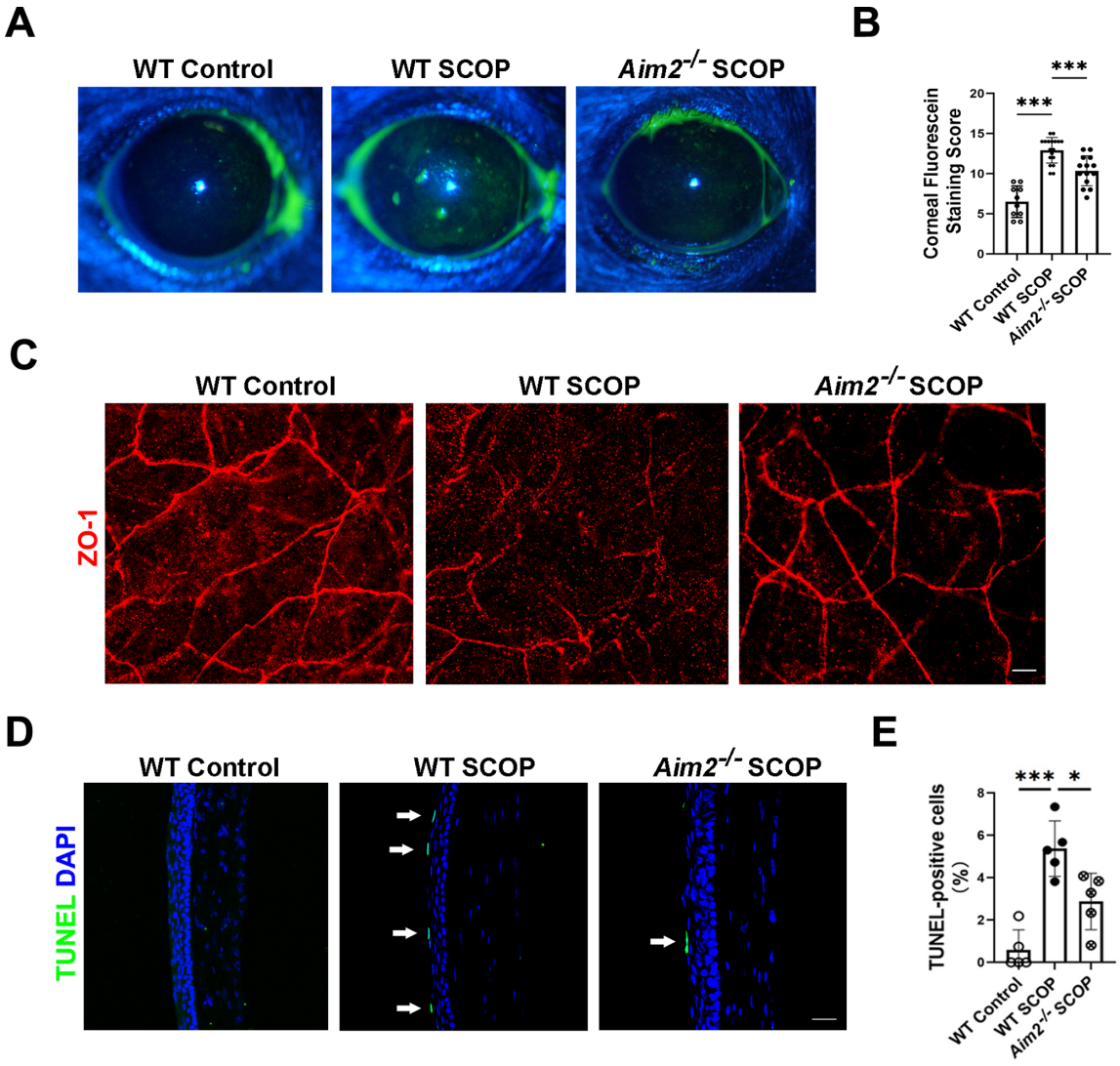

Figure 4. *Aim2* deficiency alleviates corneal epithelial barrier disruption in SCOP-induced DED. (**A**) Representative corneal fluorescein staining images at five days after induction of dry eye with SCOP in WT and *Aim2*$^{-/-}$ mice. WT mice administered with saline solution used as a control. (**B**) Quantification of corneal fluorescein staining scores of WT control (n = 10), WT SCOP (n = 18), and *Aim2*$^{-/-}$ SCOP (n = 14). (**C**) Representative images of whole mounts of cornea immunostained for ZO-1 (*red*). *Scale bar*: 5 µm. (**D**) Representative images for TUNEL staining of cornea in the WT control group, WT SCOP group, and *Aim2*$^{-/-}$ SCOP group. (**E**) The quantification of TUNEL-positive cells by calculating the percentage of TUNEL-positive cells compared to the total number of corneal epithelial cells (n = 5). *$P < 0.05$, ***$P < 0.001$.

Aim2 Deficiency Suppresses Macrophage Infiltration and Inhibits N-GSDMD and IL18 Production in The LG of SCOP-induced DED

To explore the underlying pathological mechanisms of AIM2 in DED, we analyzed macrophage infiltration in LG using immunohistochemistry for macrophage marker F4/80. The results showed comparable infiltration of macrophages in WT and *Aim2*$^{-/-}$ mice under normal conditions (Supplementary Fig. S1). After the administration of SCOP for 5 days, WT mice showed increased macrophage infiltration in the LG, and these macrophages moved around the atrophic acini and ducts (Figs. 6A, 6B). Moreover, we observed that the *Aim2*$^{-/-}$ SCOP group exhibited less macrophage infiltration than WT SCOP group (Figs. 6A, 6B). Immunoblots showed that caspase-1 proteolytic cleavage (P10) was significantly increased in the LG of the WT SCOP group; however, it was attenuated in *Aim2*$^{-/-}$ SCOP group (Figs. 6C, 6D). Active caspase-1-mediated cleavage of GSDMD leads to the liberation of its N-terminal domain, which forms pores in the plasma membrane and subsequently initiates pyroptotic cell death.[10,30,31] Our data verified that N-GSDMD was significantly increased in the LG of WT SCOP group compared with that in the control. However, the deletion of AIM2 significantly blocked the cleavage of GSDMD (Figs. 6C, 6D). To confirm whether *Aim2* deficiency reduces the release of aberrant DNA, aberrant DNA in LG of the *Aim2*$^{-/-}$ SCOP groups was evaluated by immunostaining. As shown in Supplementary Figure S2, there was no significant difference in aberrant DNA in the LG between the WT and *Aim2*$^{-/-}$ SCOP groups. Moreover, the activation of caspase-1 cleaves pro-IL-1β and pro-IL-18 into a mature form.[10] Deletion of

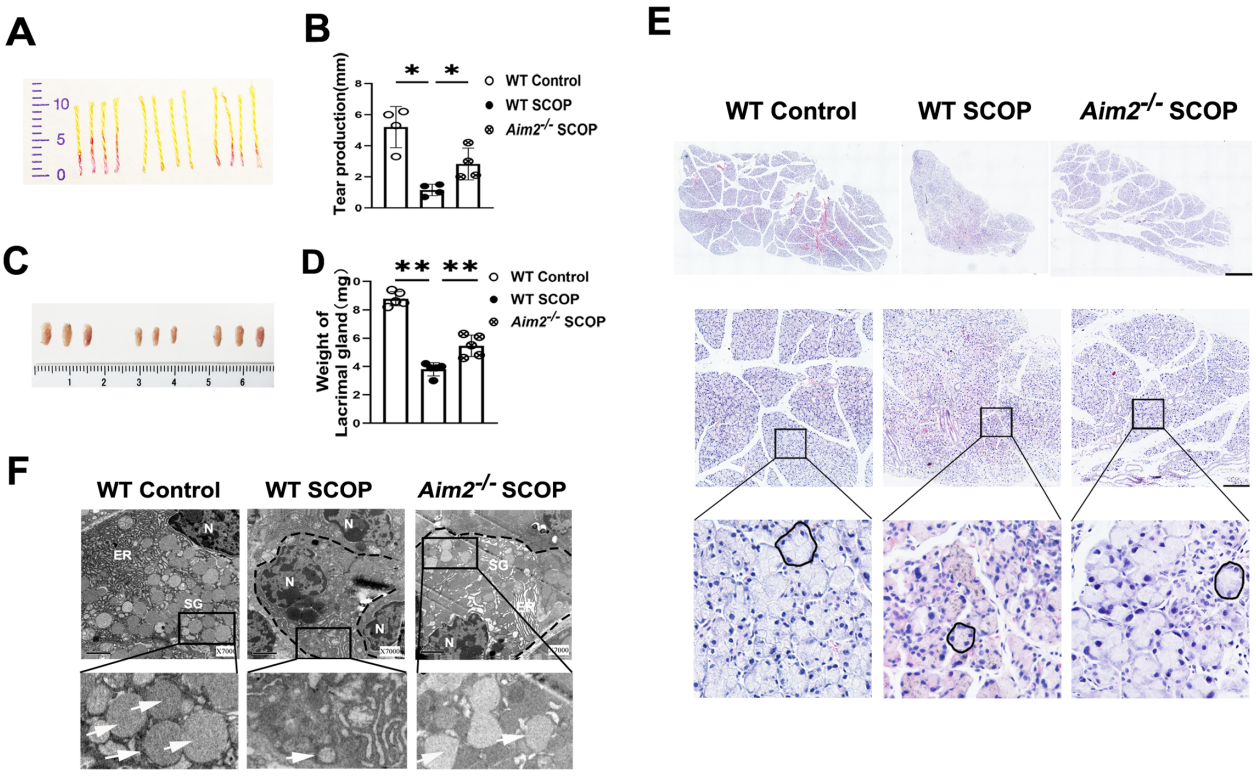

Figure 5. *Aim2* deficiency ameliorates lacrimal gland destruction and secretory dysfunction in SCOP–induced dry eye model. (**A**) Aqueous tear production assessed by phenol red thread test in WT control, WT SCOP, and *Aim2*$^{-/-}$ SCOP. (**B**) Quantification of the tear production by the length of wet (*red*) portion of thread in **A**. *$P < 0.05$. (C) Macro images of lacrimal glands in WT control, WT SCOP, and *Aim2*$^{-/-}$ SCOP. (**D**) Comparison of lacrimal gland weight. **$P < 0.01$. (**E**) Representative scans of lacrimal gland sections stained with HE in WT control, WT SCOP, and *Aim2*$^{-/-}$ SCOP group. *Circles* mark acinar cells. *Scale bar* of images in the upper row: 500 µm. *Scale bar* of images in the middle row: 200 µm. (**F**) Representative transmission electron microscopy images of lacrimal glands in WT control, WT SCOP, and *Aim2*$^{-/-}$ SCOP group. *White arrows* mark secretory granules. N, nuclei; ER, endoplasmic reticulum; SG, secretory granules.

Aim2 suppressed the increase of IL-18 in the LG of SCOP group. However, the levels of IL-1β were similar in LG of the WT and *Aim2*$^{-/-}$ SCOP groups (Figs. 6C–E).

Discussion

In the development of DED, disruption of tear film homeostasis is fundamental process.[1] The investigations of pathogenic mechanisms help drive therapeutic approaches to restore tear film and ocular surface homeostasis in DED. Owing to the main pathologic location and easy accessibility, the contribution of inflammasomes activation to the development of DED is mostly focused on the corneal epithelium.[2–5] However the precise role of inflammasomes in the LG of DED has rarely been elucidated. In this study, we showed that AIM2 inflammasomes regulates dry eye process by affecting LG functions. We noted the presence of markedly aberrant DNA accumulation accompanied by increased AIM2 levels in the LG of SCOP-induced DED. Although AIM2 is not essential for ocular surface homeostasis under normal conditions, *Aim2* deficiency alleviated LG destruction and corneal epithelium defects in the experimental DED model. Furthermore, *Aim2* deficiency suppressed macrophage infiltration and reversed the increased IL-18 and cleavage of pyroptosis executor GSDMD in the LG of SCOP-induced DED.

Sjögren's syndrome (SS), an autoimmune disorder that primarily targets the salivary and lacrimal glands, causes dry mouth and the most severe aqueous tear–deficient DED.[32] In the salivary epithelia of patients with SS, marked cytoplasmic accumulations of damaged genomic DNA that triggered AIM2 activation was observed.[33] However, the accumulations of aberrant DNA in LG of SS have not been characterized. Our study provides evidence suggesting aberrant DNA accumulations accompanied by increased AIM2 level in the LG of SCOP-induced DED, and deletion of AIM2 could alleviate LG destruction and secretory dysfunction. The contribution of AIM2 to SS-associated DED need to be further characterized. Several mouse models of SS have been developed, including CD25 knockout strains, and C57BL/6.NOD-*Aec1Aec2 (Aec)* mice, have been used to study the pathogenic mechanisms of LG destruction and secretory dysfunction in SS.[34,35] Unlike that administration of SCOP in eight-week-old female mice for five days can induce significant dry eye manifestation,[26,36] these spontaneously SS mouse models generally need several months to develop SS-like disease manifestations.[34,35] Further investigations are needed to determine the contribution of the AIM2 to the onset and severity of dacryoadenitis in these spontaneously SS mouse models.

Macrophages play an essential role in the innate immune response through phagocytosis of pathogens and cellular debris, and provision of inflammatory cytokines.[37] Our findings showed an increased infiltration of macrophages in the LG of SCOP-induced DED, which is consistent with a previous study.[38] Moreover, these macrophages moved

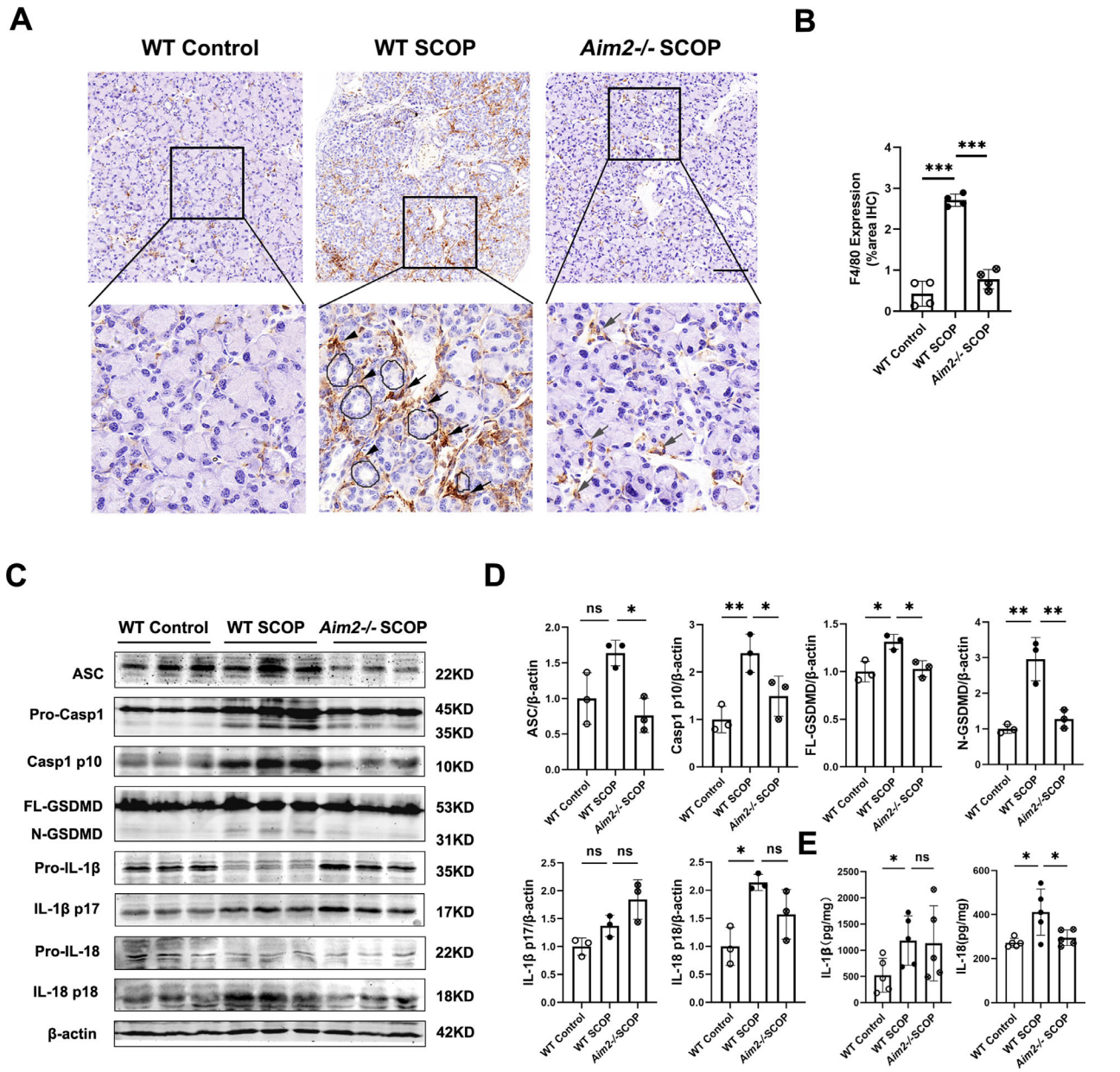

Figure 6. Aim2 deficiency abrogates increased macrophage infiltration and GSDMD cleavage in SCOP-induced DED. (**A**) Immunohistochemistry for the macrophage marker F4/80 in LG of WT control, WT SCOP, and *Aim2*$^{-/-}$ SCOP. Positive cells are stained *brown*. The *black arrows* mark F4/80-positve macrophages surrounding atrophic acini. The *black arrowbeads* mark macrophages surrounding ducts. The *gray arrows* mark macrophages in LG of the *Aim2*$^{-/-}$ SCOP group. *Scale bar*: 100 µm. (**B**) Quantitative analyses of F4/80 immunohistochemistry in LG of the WT control, WT SCOP, and *Aim2*$^{-/-}$ SCOP group. The average percentages of macrophage infiltration areas were quantified in three random vision fields of one sample (1 sample = 1 mouse), which were calculated by ImageJ software (n = 4 samples/group). ***$P < 0.001$. Immunoblot analysis (**C**) and quantification of band intensity (**D**) of AIM2 inflammasomes-related protein and β-actin in lacrimal glands of WT control, WT SCOP, and *Aim2*$^{-/-}$ SCOP. Control group was taken as the calibrator (n = 3). (**E**) Analyses of IL-1β and IL-18 in lacrimal glands of WT control, WT SCOP, and *Aim2*$^{-/-}$ SCOP by ELISA (n = 5). *$P < 0.05$, **$P < 0.01$, ***$P < 0.001$. ns, not significant.

around the atrophic acini and ducts in the WT SCOP group. Infiltration of macrophages expressing high levels of IL-18 was observed in the salivary glands of patients with primary SS, which contributed to the expansion of infiltrative injuries.[39] Our results showed the increased expression of IL-18 paralleled increased infiltration of macrophages in SCOP-induced DED, which appear to play active roles in LG destruction and secretory dysfunction. Furthermore, we determined that *Aim2* deficiency could suppress infiltration of macrophages into the LG and decrease the expression of IL-18 in SCOP-induced DED. Previous studies have suggested AIM2 governs macrophage infiltration to promote inflammation and tissue injury, and AIM2-deficient mice exhibited decreased infiltration of macrophages and associated histopathological findings in a polyarthritis-like disease model or unilateral ureteral obstruction model.[40,41] Given the importance of *Aim2* regulation in recruitment of macrophage, *Aim2* might influence the LG inflammation through recruitment of macrophages in SCOP-induced DED. Meanwhile, our results showed that the levels of IL-1β in LG

of the *Aim2*$^{-/-}$ SCOP were similar as compared to WT SCOP groups, suggesting that *Aim2* deficiency does not ameliorate LG dysfunction via IL-1β-mediated inflammation. It seems that a more complex network regulates IL-1β in the LG of SCOP-induced DED, which needs further investigation in the future.

Our investigation showed that AIM2 inflammasome activation contributed to caspase-1-mediated GSDMD cleavage in the LG of SCOP-induced DED, accompanied by decreased tear production. GSDMD has been implicated in tear reduction in experimental DED.[2] Further in-depth investigations are required to clarify whether *Aim2* deficiency ameliorates ocular surface disorder via GSDMD-mediated tear reduction. GSDMD, a common downstream protein of different inflammasomes, is activated by the AIM2 inflammasome in LG, and by TLR4-CASP8-NLRP12/NLRC4 inflammasome[2] and NLRP3 inflammasome[3] in corneal epithelium of experimental DED. Thus the pharmacological targeting of GSDMD may be beneficial for treating DED.

In conclusion, this study provides evidence that deletion of AIM2 alleviates LG damage and tear reduction, subsequently reducing corneal epithelia defects in SCOP-induced DED. AIM2 might influence the LG inflammation through recruitment of macrophages and cleavage of the pyroptosis executor GSDMD in SCOP-induced DED. These findings provide a novel mechanistic explanation for the inflammasome status in the LG of DED, as well as potential therapeutic targets to modulate LG inflammation in DED.

Acknowledgments

Supported by the National Natural Science Foundation of China (81500699, 81970770), the Natural Science Foundation of Zhejiang Province (LY18H120007).

Disclosure: **Y. Chen**, None; **J. Pu**, None; **X. Li**, None; **L. Lian**, None; **C. Ge**, None; **Z. Liu**, None; **W. Wang**, None; **L. Hou**, None; **W. Chen**, None; **J. Li**, None

References

1. Craig JP, Nichols KK, Akpek EK, et al. TFOS DEWS II definition and classification report. *Ocul Surf*. 2017;15:276–283.
2. Chen H, Gan X, Li Y, et al. NLRP12- and NLRC4-mediated corneal epithelial pyroptosis is driven by GSDMD cleavage accompanied by IL-33 processing in dry eye. *Ocul Surf*. 2020;18:783–794.
3. Zhang J, Dai Y, Yang Y, Xu J. Calcitriol alleviates hyperosmotic stress-induced corneal epithelial cell damage via inhibiting the NLRP3-ASC-Caspase-1-GSDMD pyroptosis pathway in dry eye disease. *J Inflamm Res*. 2021;14:2955–2962.
4. Zheng Q, Ren Y, Reinach PS, et al. Reactive oxygen species activated NLRP3 inflammasomes prime environment-induced murine dry eye. *Exp Eye Res*. 2014;125:1–8.
5. Zheng Q, Ren Y, Reinach PS, et al. Reactive oxygen species activated NLRP3 inflammasomes initiate inflammation in hyperosmolarity stressed human corneal epithelial cells and environment-indu dry eye patients. *Exp Eye Res*. 2015;134:133–140.
6. Schroder K, Tschopp J. The inflammasomes. *Cell*. 2010;140:821–832.
7. Rathinam VA, Fitzgerald KA. Inflammasome Complexes: Emerging Mechanisms and Effector Functions. *Cell*. 2016;165:792–800.
8. Liston A, Masters SL. Homeostasis-altering molecular processes as mechanisms of inflammasome activation. *Nat Rev Immunol*. 2017;17:208–214.
9. Xue Y, Enosi Tuipulotu D, Tan WH, Kay C, Man SM. Emerging activators and regulators of inflammasomes and pyroptosis. *Trends Immunol*. 2019;40:1035–1052.
10. Van Opdenbosch N, Lamkanfi M. Caspases in cell death, inflammation, and disease. *Immunity*. 2019;50:1352–1364.
11. Martinon F, Burns K, Tschopp J. The inflammasome: A molecular platform triggering activation of inflammatory caspases and processing of proIL-beta. *Mol Cell*. 2002;10:417–426.
12. Lu F, Lan Z, Xin Z, et al. Emerging insights into molecular mechanisms underlying pyroptosis and functions of inflammasomes in diseases. *J Cell Physiol*. 2020;235:3207–3221.
13. Jin T, Perry A, Smith P, Jiang J, Xiao TS. Structure of the absent in melanoma 2 (AIM2) pyrin domain provides insights into the mechanisms of AIM2 autoinhibition and inflammasome assembly. *J Biol Chem*. 2013;288:13225–13235.
14. Burckstummer T, Baumann C, Bluml S, et al. An orthogonal proteomic-genomic screen identifies AIM2 as a cytoplasmic DNA sensor for the inflammasome. *Nat Immunol*. 2009;10:266–272.
15. Fernandes-Alnemri T, Yu JW, Datta P, Wu J, Alnemri ES. AIM2 activates the inflammasome and cell death in response to cytoplasmic DNA. *Nature*. 2009;458:509–513.
16. Rathinam VA, Jiang Z, Waggoner SN, et al. The AIM2 inflammasome is essential for host defense against cytosolic bacteria and DNA viruses. *Nat Immunol*. 2010;11:395–402.
17. Wang B, Bhattacharya M, Roy S, Tian Y, Yin Q. Immunobiology and structural biology of AIM2 inflammasome. *Mol Aspects Med*. 2020;76:100869.
18. Lammert CR, Frost EL, Bellinger CE, et al. AIM2 inflammasome surveillance of DNA damage shapes neurodevelopment. *Nature*. 2020;580:647–652.
19. Roth S, Cao J, Singh V, et al. Post-injury immunosuppression and secondary infections are caused by an AIM2 inflammasome-driven signaling cascade. *Immunity*. 2021;54:648–659.e648.
20. Lian Q, Xu J, Yan S, et al. Chemotherapy-induced intestinal inflammatory responses are mediated by exosome secretion of double-strand DNA via AIM2 inflammasome activation. *Cell Res*. 2017;27:784–800.
21. Tibrewal S, Sarkar J, Jassim SH, et al. Tear fluid extracellular DNA: Diagnostic and therapeutic implications in dry eye disease. *Invest Ophthalmol Vis Sci*. 2013;54:8051–8061.
22. Sonawane S, Khanolkar V, Namavari A, et al. Ocular surface extracellular DNA and nuclease activity imbalance: A new paradigm for inflammation in dry eye disease. *Invest Ophthalmol Vis Sci*. 2012;53:8253–8263.
23. Kumari P, Russo AJ, Shivcharan S, Rathinam VA. AIM2 in health and disease: Inflammasome and beyond. *Immunol Rev*. 2020;297:83–95.
24. Li H, Li Y, Song C, et al. Neutrophil extracellular traps augmented alveolar macrophage pyroptosis via AIM2 inflammasome activation in LPS-induced ALI/ARDS. *J Inflamm Res*. 2021;14:4839–4858.
25. Lemp MA. Report of the National Eye Institute/Industry Workshop on Clinical Trials in Dry Eyes. *CLAO J*. 1995;21:221–232.
26. Chen Y, Chauhan SK, Lee HS, et al. Effect of desiccating environmental stress versus systemic muscarinic AChR blockade on dry eye immunopathogenesis. *Invest Ophthalmol Vis Sci*. 2013;54:2457–2464.
27. Dawson L, Tobin A, Smith P, Gordon T. Antimuscarinic antibodies in Sjogren's syndrome: Where are we, and where are we going? *Arthritis Rheum*. 2005;52:2984–2995.

28. Toth-Molnar E, Ding C. New insight into lacrimal gland function: Role of the duct epithelium in tear secretion. *Ocul Surf*. 2020;18:595–603.
29. Pflugfelder SC, Stern ME. Biological functions of tear film. *Exp Eye Res*. 2020;197:108115.
30. Wang K, Sun Q, Zhong X, et al. Structural mechanism for GSDMD targeting by autoprocessed caspases in pyroptosis. *Cell*. 2020;180:941–955.e920.
31. Liu X, Zhang Z, Ruan J, et al. Inflammasome-activated gasdermin D causes pyroptosis by forming membrane pores. *Nature*. 2016;535:153–158.
32. Bjordal O, Norheim KB, Rodahl E, Jonsson R, Omdal R. Primary Sjogren's syndrome and the eye. *Surv Ophthalmol*. 2020;65:119–132.
33. Vakrakou AG, Svolaki IP, Evangelou K, Gorgoulis VG, Manoussakis MN. Cell-autonomous epithelial activation of AIM2 (absent in melanoma-2) inflammasome by cytoplasmic DNA accumulations in primary Sjogren's syndrome. *J Autoimmun*. 2020;108:102381.
34. Bian F, Barbosa FL, Corrales RM, et al. Altered balance of interleukin-13/interferon-gamma contributes to lacrimal gland destruction and secretory dysfunction in CD25 knockout model of Sjogren's syndrome. *Arthritis Res Ther*. 2015;17:53.
35. You IC, Bian F, Volpe EA, de Paiva CS, Pflugfelder SC. Age-related conjunctival disease in the C57BL/6.NOD-Aec1Aec2 mouse model of Sjogren syndrome develops independent of lacrimal dysfunction. *Invest Ophthalmol Vis Sci*. 2015;56:2224–2233.
36. Pitcher JD, 3rd, De Paiva CS, Pelegrino FS, et al. Pharmacological cholinergic blockade stimulates inflammatory cytokine production and lymphocytic infiltration in the mouse lacrimal gland. *Invest Ophthalmol Vis Sci*. 2011;52:3221–3227.
37. Varol C, Mildner A, Jung S. Macrophages: Development and tissue specialization. *Ann Rev Immunol*. 2015;33:643–675
38. Xiao B, Wang Y, Reinach PS, et al. Dynamic ocular surface and lacrimal gland changes induced in experimental murine dry eye. *PloS One*. 2015;10:e0115333.
39. Manoussakis MN, Boiu S, Korkolopoulou P, et al. Rates of infiltration by macrophages and dendritic cells and expression of interleukin-18 and interleukin-12 in the chronic inflammatory lesions of Sjogren's syndrome: Correlation with certain features of immune hyperactivity and factors associated with high risk of lymphoma development. *Arthritis Rheum*. 2007;56:3977–3988.
40. Komada T, Chung H, Lau A, et al. Macrophage uptake of necrotic cell DNA activates the AIM2 inflammasome to regulate a proinflammatory phenotype in CKD. *J Am Soc Nephrol*. 2018;29:1165–1181.
41. Jakobs C, Perner S, Hornung V. AIM2 drives joint inflammation in a self-DNA triggered model of chronic polyarthritis. *PloS One*. 2015;10:e0131702.

Investigative Ophthalmology & Visual Science